Arch. Metall. Mater. **66** (2021), 4, 997-1000

DOI: 10.24425/amm.2021.136413

HYUN-KUK-PARK[1], IK-HYUN-OH[1], JU-HUN-KIM[1,2], SUNG-KIL-HONG[2], JEONG-HAN LEE[1,2*]

CONSOLIDATION AND OXIDATION OF ULTRA FINE WC-Co-HfB_2 HARD MATERIALS BY SPARK PLASMA SINTERING

In this study, a novel composite was fabricated by adding the Hafnium diboride (HfB_2) to conventional WC-Co cemented carbides to enhance the high-temperature properties while retaining the intrinsic high hardness. Using spark plasma sintering, high density (up to 99.4%) WC-6Co-(1, 2.5, 4, and 5.5 wt. %) HfB_2 composites were consolidated at 1300°C (100°C/min) under 60 MPa pressure. The microstructural evolution, oxidation layer, and phase constitution of WC-Co-HfB_2 were investigated in the distribution of WC grain and solid solution phases by X-ray diffraction and FE-SEM. The WC-Co-HfB_2 composite exhibited improved mechanical properties (approximately 2,180.7 kg/mm^2) than those of conventional WC-Co cemented carbides. The high strength of the fabricated composites was caused by the fine-grade HfB_2 precipitate and the solid solution, which enabled the tailoring of mechanical properties.

Keywords: WC cemented carbide, hafnium diboride, spark plasma sintering, oxidation, mechanical property

1. Introduction

Tungsten carbide-cobalt (WC-Co) cemented carbides are widely used in cutting tools for machining of hard materials, which require high strength, thermal stability, and wear resistance [1-2]. However, WC-Co cemented carbides undergo severe electrochemical corrosion and oxidation above 400°C [3,4], which reduce the life of cutting tools because of abrasion between the cutting edge and surface [3]. To overcome this problem, novel carbide composites with transition metal diborides, such as hafnium diboride (HfB_2), titanium diboride (TiB_2), and zirconium diboride (ZrB_2), have been proposed. HfB_2 has the highest oxidation resistance among diborides owing to its high melting point and other thermal properties [3]. Furthermore, its metal boride phase acts as a grain growth inhibitor [2] for carbide grains during the consolidation of powders.

This study focuses on the improvement of the sintering kinetics, mechanical properties, and high-temperature oxidation resistance of WC-Co cemented carbide by the addition of HfB_2. WC-Co-HfB_2 powders were densely consolidated by spark plasma sintering (SPS). The phase constitution and densification behavior of the WC-Co-HfB_2 sintered compacts were investigated. Furthermore, the effect of HfB_2 on the oxidation behavior was explored based on the microstructure and quantitative profiling within WC-Co-HfB_2 hard materials.

2. Experimental

WC (≤0.5 μm), Co (≤10.0 μm), and HfB_2 (≤44.0 μm) powders were used as starting materials; they were synthesized by planetary ball milling with WC balls under a ball-to-powder ratio of 2:1 for 12 h in ethanol medium at 250 rpm. Different powder compositions of WC-6Co-HfB_2 were prepared using 1, 2.5, 4, and 5.5 wt. % HfB_2.

The synthesized powders were consolidated by SPS at a sintering temperature of 1300°C and heating rate of 100°C/min under an applied pressure of 60 MPa. The sintering behavior during densification and consolidation was investigated by the macroscopic shrinkage strain using Eq. (1).

$$\varepsilon_s{}^m = \left(\frac{\Delta L}{L_0}\right)^m = -\left(\frac{X}{2D}\right)^2,\ \rho_S = \rho_G \Big/ \left(1-\frac{\Gamma L}{L_0}\right)^3 \tag{1}$$

where, ε_s is the densification strain, m is the sintering exponent, ΔL is the shrinkage displacement, L_0 is the original length of the

[1] KOREA INSTITUTE OF INDUSTRIAL TECHNOLOGY, SMART MOBILITY MATERIALS AND COMPONENTS R&D GROUP, 6, CHEOMDAN-GWAGIRO 208-GIL, BUK-GU, GWANG-JU, 61012, KOREA
[2] CHONNAM NATIONAL UNIVERSITY, MATERIALS SCIENCE & ENGINEERING, 77, YONG-BONGRO, BUK-GU, GWANG-JU, 61186, KOREA
* Corresponding author: ljh88@kitech.re.kr

green body, ρ_S is the sintered relative density, ρ_G is the density of the green body, and (X/2D) is the neck-to-particle diameter ratio.

The phase constitutions of the powders and sintered materials were investigated by X-ray diffraction (XRD) with CuKα radiation ($\lambda = 0.154$ nm). The average crystallite size and microstrain were characterised by a Willamson-Hall plot using Eq. (2).

$$D = \frac{k\lambda}{\beta_{hkl}\cos\theta}\ ,\ \varepsilon = \frac{\beta_{hkl}}{4\tan\theta} \tag{2}$$

where D is the crystallite size, k is the Scherrer's constant (0.9), and λ is the wavelength of CuKα radiation. Instrumental broadening is expressed as β_{hkl} of the corrected value derived from the microstrain (ε).

WC-Co-HfB_2 composites were treated in a heat furnace in a ZrO_2 crucible at temperatures up to 1000°C (10°C/min) to investigate the oxidation behavior. The microstructures of WC-Co-HfB_2 were explored by field emission scanning electron microscopy (FE-SEM) analysis of the cross sections with an oxidation/matrix interface. The effect of HfB_2 on oxidation resistance was observed by scanning electron microscopy/energy dispersive X-Ray spectroscopy (SEM-EDS) analysis.

The mechanical properties of the WC-Co-HfB_2 hard materials were measured by Vickers hardness test with a load of 20 kg·f applied for 15 s. In addition, fracture toughness (K_{IC}) was obtained by the Antis formula given in Eq. (3).

$$K_{IC} = 0.016\left(\frac{E}{H}\right)^{1/2} P / C^{3/2} \tag{3}$$

where E is the elastic modulus, H is the hardness, P is the applied load, and C is the length of crack propagation.

3. Results and discussion

Figure 1 shows the macroscopic shrinkage displacement and densification strain of the WC-Co-HfB_2 sintered compacts. The relative densities of all the compacts were above 98.8% up to 1300°C (Fig. 1(a)) (6Co: 100.0%, 1HfB_2: 99.4%, 2.5HfB_2: 99.3%, 4HfB_2: 99.1%, and 5.5HfB_2: 98.8%). The densification behavior was divided into stage I (600-800°C) and stage II (800-1300°C), with reference to their shrinkage displacement based on the temperature at which the intergranular wetting of WC by Co-binder in a metastable liquid state. As the amount of HfB_2 increased, rapid shrinkage at lower sintering temperatures was observed. Lower densification temperatures were promoted by using HfB_2 dispersants as a grain growth inhibitor [6] at the grain boundaries before Co wetting. Therefore, the nominal sintering kinetics with the densification strain rate of the WC-Co-HfB_2 sintered compacts for stages I and II depend on their sintering exponent (ε_s) and activation energy (Q) (*see* Fig. 1(b)). The sintering exponent is a function of the diffusion path, wherein the slope (mQ) refers to the effective activation energy for lattice (LD) and grain boundary (GB) diffusion [5]. Depending on the diffusion path, LD diffusion is promoted at a relatively low temperature [5], that is, in stage I, where the Q_I value shows a significant increase for above 4.0 wt. % HfB_2. This is attributed to the distortion of the WC lattice structure because of the HfB_2 interfacial dispersants. On the other hand, in stage II, Q_{II} is related to GB diffusion in WC, where the HfB_2 hardly contributes to solid-state diffusion (e.g. GB recreation and elimination of isolated open pores) owing to its low Q value. This result suggests that HfB_2 may affect the wettability and act as an obstacle to the diffusion path of Co in the stage II of sintering.

Figure 2 shows the structural evolution, starting from the sintered compact to the oxidized WC-Co-HfB_2 hard materials. In Fig. 2(a), the decrease in WC lattice parameters from 2.517 to 2.499 Å to increasing HfB_2 content indicates lattice distortion by the formation of solid solutions. In addition, the intensity of the basal plane (001) of WC was significantly decreased by hard HfB_2 dispersants which interfered with the coherent relationship of hcp-WC(001)//fcc-Co(111) interface [1]. Hence, they act as obstacles to the dislocations and the basal twins that could cause plastic deformation [6]. The phase composition of the oxidized WC-Co-HfB_2 hard materials is shown in Fig. 2(b). Several oxi-

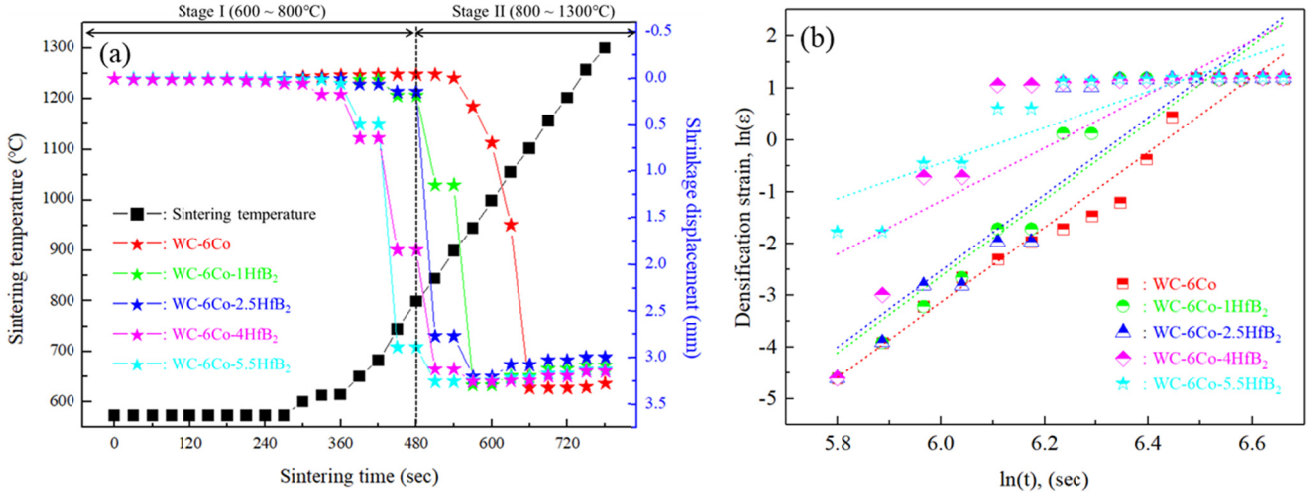

Fig. 1. Sintering behaviors of WC-Co-HfB_2 hard materials: (a) schematic of macroscopic shrinkage displacement and (b) densification strain-sintering time curve with a sintering exponent

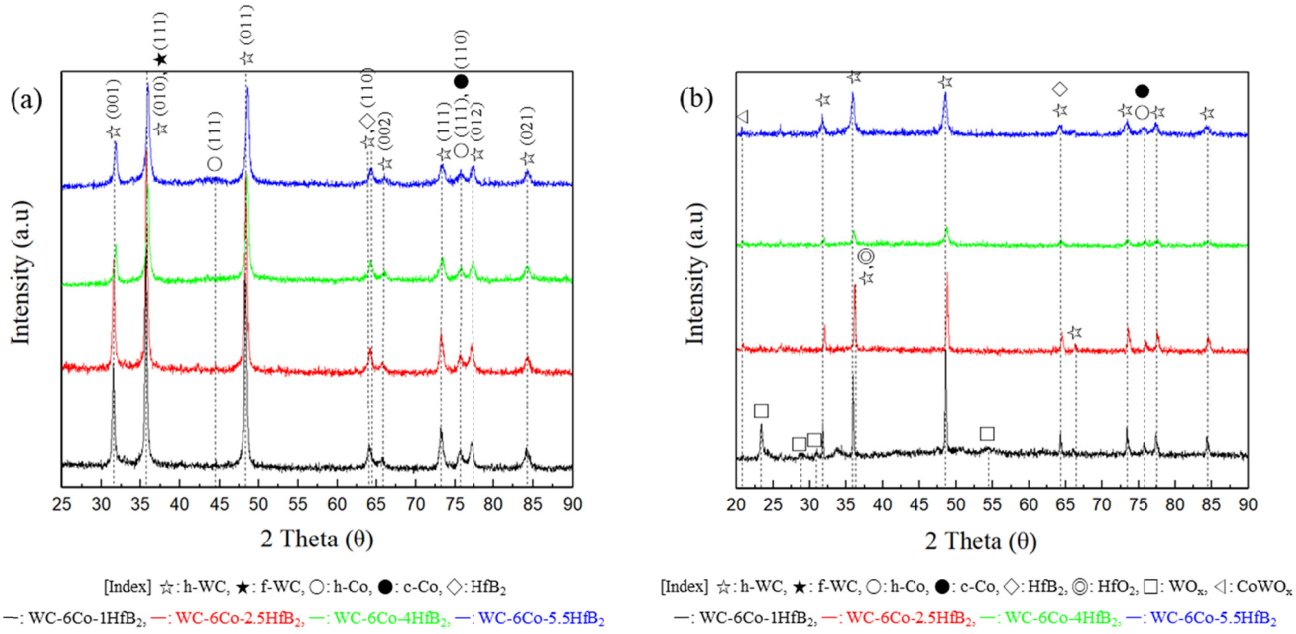

Fig. 2. XRD patterns of WC-Co-HfB_2 hard materials: (a) as sintered-bodies and (b) for oxidized at 1000°C

dation reactions occurred in the WC and Co phases (WO_x and $CoWO_x$), and a layer of partially oxidized HfO_2 and residual carbon was observed in the specimen containing 2.5 wt. % HfB_2 [7]. The oxidized phases were consistent with the study by C. Bagnall et al. [8], which states that concurrent oxidation of WC and Co can be achieved above 570°C with a thin WO_3 (mainly) and $CoWO_4$ layer.

Figure 3 shows the microstructure of the oxide/matrix layer of the WC-Co-HfB_2 hard materials after exposure to 1000°C. As shown in Fig. 3(b), a sharp decrease in the oxygen (O) peak was observed, which was attributed to the localized oxidation resistance owing to the formation of the HfO_2 passivation layer. This oxidation resistance layer has been reported [5] to provide a continuous protective layer below ~1100°C. However, Fig. 3(c) and (d) show that oxidation, slightly increased compared to that in Fig. 3(b). This is attributed to the generation of CO_2 inside the partially oxidized layer through a reaction with residual carbon by Eq. (4). In addition, the formation of CO_2 facilitated cracking as the oxide grew at the WC/Co interface, suggesting that its formation is favored over that of WO_3 ($\Delta G_{r,\,1000°C} = -1022.285$ kJ/mol) at an equal temperature according to the Eq. (4).

$$HfO_2(s) + 3C(s) \rightarrow HfC(s) + 2CO(g),$$
$$\Delta G_{r,1000°C} = -423.46 \text{ kJ/mol} \quad (4)$$

As the results of integral area for the oxygen (O) peaks are believed to the highest oxidation resistance effect at the 2.5% addition HfB_2 (*see* Fig. 3(e)). This effect is attributed to the oxide layer having the lowest thickness (~300 μm) compared to others due to the formation of the HfO_2 protective layer.

Table 1 shows the mechanical properties of WC-Co-HfB_2 hard materials. The average hardness increases from 1783.5 to 2180.7 kg/mm^2, whereas the average fracture toughness

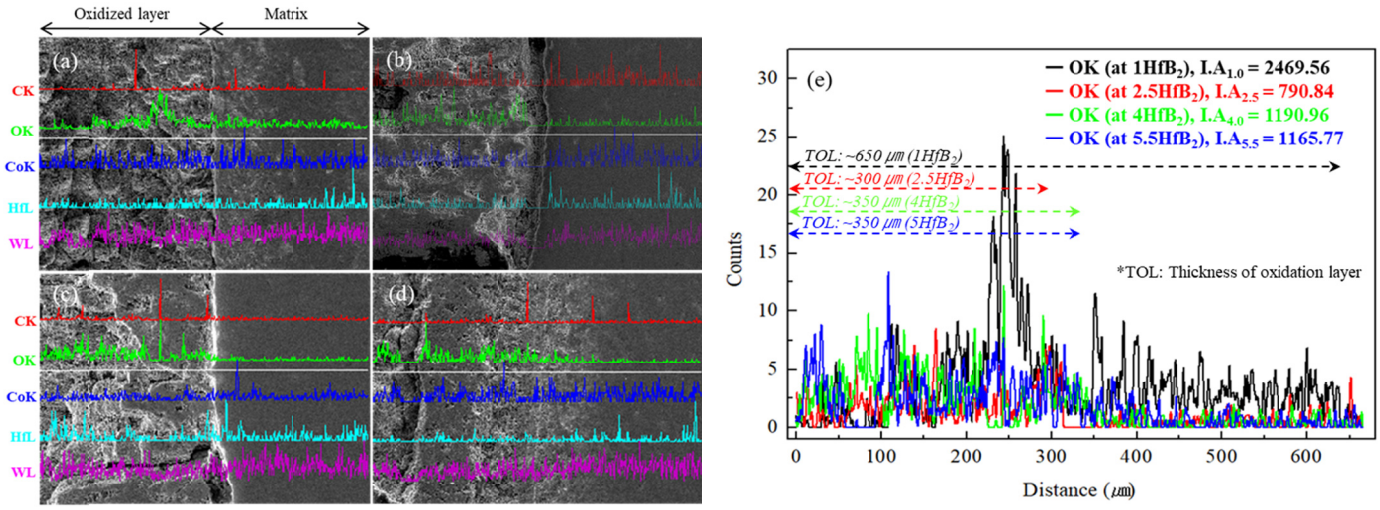

Fig. 3. Microstructure of cross section with oxidation layer/matrix for WC-Co-HfB_2 hard materials: (a) 1HfB_2, (b) 2.5HfB_2, (c) 4HfB_2, (d) 5.5HfB_2, and (e) quantitative data of oxygen (O) elements line profile from oxidation layer to matrix

TABLE 1

Comparison of mechanical and structural properties of WC-Co-HfB_2 hard materials

Specimens	Properties				
	Hardness (kg/mm^2)	Fracture toughness ($MPa \cdot m^{1/2}$)	Crystallite size (μm)	Microstrain	Relative density (%)
WC-6Co	1783.5	13.7	0.37	0.18	100.0
WC-6Co-1HfB_2	1933.3	7.9	0.37	0.24	99.4
WC-6Co-2.5HfB_2	2123.6	6.6	0.34	0.24	99.3
WC-6Co-4HfB_2	2140.3	6.5	0.29	0.26	99.1
WC-6Co-5.5HfB_2	2180.7	6.3	0.27	0.31	98.8

decreases from 13.7 to 6.3 $MPa \cdot m^{1/2}$. Grain refinement with the addition of HfB_2 was confirmed (from 0.37 to 0.27 μm), and a high internal strain ($\varepsilon = 0.31$) of the lattice was obtained, which indicated solid solution strengthening.

4. Conclusions

The sintering kinetics suggested that HfB_2 acts as an obstacle to the diffusion path of Co at the solid/liquid interface. Oxidation behavior was determined by the formation of an oxide-resistant layer (HfO_2), wherein the saturation of HfB_2 was caused by continuous oxidation at the interface matrix/binder. The highest oxidation resistance is exhibited at the 2.5 wt.% HfB_2 due to the formation of the HfO_2 protective layer. The specimen containing 5.5 wt.% HfB_2 exhibited the highest hardness (2,180.7 kg/mm^2) owing to the effects of grain refinement and solid solution strengthening.

Acknowledgments

This study has been conducted with the support of the Korea Institute of Industrial Technology (KITECH), Production Industry Leading Core Technology Developement Project as the "Development of an on-site facility attached cryogenic machining integrated system (KITECH EH-21-0010)".

REFERENCES

[1] J.H. Lee, I.H. Oh, J.H. Jang, S.K. Hong, H.K. Park, J. Alloys Compd. **786**, 1-10 (2019).

[2] J. Garcia, V.C. Cipres, A. Blomqvist, B. Kaplan, Int. J. Refract. Met. Hard Mater. **80**, 40-68 (2019).

[3] S.A. Shalmani, M. Sobhani, O. Mirzaee, M. Zakeri, Ceram. Int. **46** (16), 25106-25112 (2020).

[4] M.D. Brut, D. Tetard, C. Tixier, C. Faure, E. Chabas, 10th International Conference of the European Ceramic Society, Berlin, 1315-1320 (2007).

[5] A.K. Kumar, K. Kurokawa, Books: Tungsten carbide – Processing and applications, chapter 2: Spark plasma sintering of ultrafine WC powders: A combined kinetic and microstructural study (2012).

[6] R.G. Crookes, B. Marz, H. Wu, Mater. Des. **187**, 108360 (2020).

[7] C. Bargeron, R. Benson, R. Newman, A.N. Jette, T.E. Phillips, Mater. Sci. (1993).

[8] C. Bagnall, J. Capo, W.J. Moorhead, Metallography Microstructure Analysis **7**, 661-679 (2018).